PHYSICAL REVIEW B, VOLUME 65, 201201(R)

Coherent response of spin-orbit split-off excitons in InP: Isolation of many-body effects through interference

K. C. Hall, G. R. Allan,* and H. M. van Driel
Department of Physics, University of Toronto, 60 St. George Street, Toronto, Ontario, Canada M5S 1A7

T. Krivosheeva
Department of Physics, University of Illinois at Chicago, Chicago, Illinois 60607

W. Pötz
Institut für Theoretische Physik, Karl-Franzens Universität Graz, Universitätsplatz 5, A-8010 Graz, Austria

(Received 27 February 2002; published 30 April 2002)

The spin-orbit split-off (SO) exciton is observed in a III-V semiconductor (InP) using spectrally resolved four-wave mixing (SR-FWM) with 1.515 eV, 35 fs pulses at 77 K. Interference between the coherent response of the SO exciton and that of electron-hole pairs in continuum states leads to frequency- and time-dependent signatures that can be directly attributed to excitation-induced dephasing (EID) of the SO exciton. Many-body effects can therefore be *isolated* from free induction decay contributions, in contrast to experiments that probe the fundamental exciton. Simulations employing the multiband Boltzmann-Bloch equations including EID effects corroborate our experimental results.

DOI: 10.1103/PhysRevB.65.201201 PACS number(s): 78.47.+p, 71.35.−y

During the past two decades, considerable effort has been dedicated to understanding the coherent response of III-V semiconductors such as GaAs,[1–14] especially in the energy region near the direct band gap where the fundamental exciton exists. Coherent spectroscopy techniques, such as femtosecond four-wave mixing (FWM), have provided considerable insight into this exciton's dynamic characteristics and the influence of a host of Coulomb-mediated effects, including local field interactions[5] and exciton-carrier scattering processes.[3,4,6,9–14] However, complex experiments have often been needed to reveal several aspects of the underlying many-body physics.[3,7,10,12–14] In contrast, little is known about the characteristics of the spin-orbit split-off (SO) exciton in the III-V semiconductors. This is perhaps not surprising since the SO exciton is hardly discernible in linear optical experiments.[15] Indirect evidence for the SO exciton has been seen in pump−continuum-probe experiments in GaAs due to conduction state energy renormalization effects,[16] although a detailed non-Markovian analysis was needed to determine the influence of the SO exciton resonance on the differential transmission spectra.[17] Here we report the observation of a *clear* signature of the SO exciton in a III-V semiconductor through measurement of its coherent response using spectrally resolved four-wave mixing (SR-FWM). The SO exciton response was studied in InP since the SO exciton energy in this system (1.532 eV at 77 K) is readily accessable by our tunable short pulse Ti:sapphire laser. Our experiments reveal that the coherent dynamics of the SO exciton differ significantly from those of the fundamental exciton since the SO exciton is *resonant* with a continuum of transitions between the heavy-hole (HH) and light-hole (LH) valence bands and the conduction band (see Fig. 1). This energy degeneracy leads to *classical* interference of the exciton and continuum polarization sources and provides a means of isolating certain many-body effects. The *interaction retardation* property of many-body related excitonic FWM signals,[5,9] such as those induced by excitation induced dephasing (EID), produces novel spectral and time-dependent characteristics through interference of the exciton emission with the optically degenerate photon echo produced by the continuum of electron-hole pair excitations. These interference effects allow Coulomb-mediated interactions to be *easily isolated* from the noninteracting optical electric field scattering contributions in FWM experiments, such as excitonic free polarization decay (FPD). This contrasts with corresponding FWM studies of the fundamental exciton, in which the similar spectral response of noninteracting, and many-body induced FWM signals complicates the interpretation of experimental results.[3,4,7,9,10,12–14] It might also be noted that apparent[19] interference effects in early FWM experiments at the fundamental exciton were more recently[3,4,9] shown to be due to EID effects themselves, and not to interference between *separate* polarization sources, as we report here. Numerical simulations of our SR-FWM experiments employing the multiband Boltzmann-Bloch equations including EID effects provide good agreement with our experimental data.

Two-pulse, degenerate SR-FWM experiments were performed at 77 K in bulk InP (band gap, $E_g = 1.414$ eV; spin-orbit valence band splitting $\Delta_0 = 108$ meV) using 35 fs (τ_p) pulses, with a full width half maximum bandwidth of 80 meV, centered at 1.515 eV (E_0). FWM spectra were measured versus pulse delay (τ) using a monochromator (0.5 meV resolution) and a photomultiplier tube. The measured signal characteristics were identical for samples of different thicknesses (0.3, 0.5 μm). The total excited carrier density generated by the two optical pulses (N_{ex}; the pulse intensity ratio was 4:1) was varied in the range 4.0×10^{16} cm^{-3} to 2.2×10^{17} cm^{-3}. Typical experimental SR-FWM results for parallel pulse polarizations ($\|$) and with $N_{ex} = 1.4\times10^{17}$ cm^{-3} appear in Fig. 2(a). The strong peak in the spectra at 1.53 eV is attributed to the coherent response of the SO exciton, while the FWM emission from carriers in continuum states appears mainly at lower photon energies.

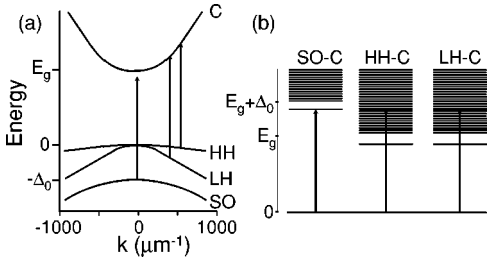

FIG. 1. (a) Schematic band structure diagram of InP. The energy axis is not to scale in order to show the valence bands more clearly. Vertical arrows indicate optical transitions resonant with the SO exciton. (b) Energy level diagram of the excitation spectrum in the exciton picture.

The most noticeable feature is the prominent dip on the low-energy side of the SO exciton peak. It is deepest in the range of pulse overlap, becoming shallower with increasing τ. The spectral positions of the dip and the SO exciton peak were found to be insensitive to changes in E_0 over the total range investigated (1.48–1.54 eV), indicating that these features arise from the optical response of the InP layer. The pulse spectrum for the data of Fig. 2 is shown in Fig. 3(a). The SR-FWM response of the SO exciton is pulse width limited versus delay, despite being spectrally narrow relative to the pulse bandwidth. The continuum emission peaks at $+20$ fs ($\approx \tau_p/2$) and thereafter decays rapidly. At low carrier densities (4.0×10^{16} cm^{-3}), the exciton feature constitutes the entire SR-FWM signal; with increasing carrier density the continuum contribution increases relative to the exciton signal. The FWM spectrum at zero pulse delay for perpendicular pulse polarizations ($\perp$) appears in Fig. 3(a),

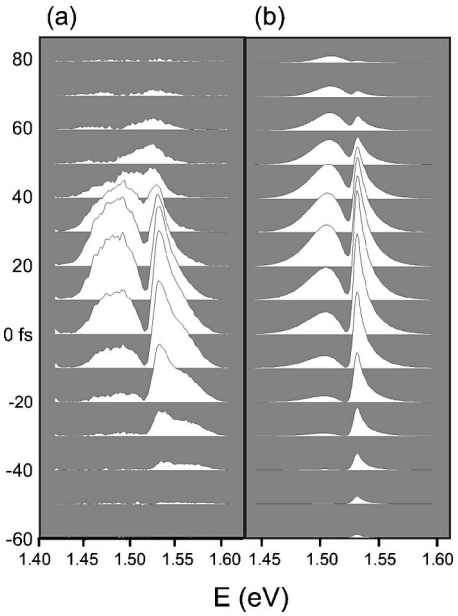

FIG. 2. (a) SR-FWM signal versus pulse delay following excitation with 1.515 eV, 35 fs optical pulses. These data were taken with parallel pulse polarizations with a total carrier density of 1.4×10^{17} cm^{-3}. (b) Calculated SR-FWM with the same excitation conditions ($N_{\rm ex}$; τ_p; E_0; incident light intensities) as in (a)

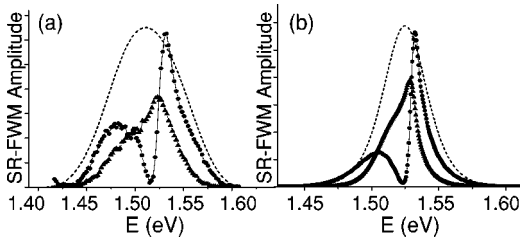

FIG. 3. (a) Experimental FWM spectrum at zero pulse delay in the $\parallel$ (circles) and $\perp$ (triangles) polarization geometries, together with the pulse spectrum (dashed curve). The excitation conditions are the same as in Fig. 2. (b) Calculated FWM spectra corresponding to the conditions in (a) along with the calculated pulse spectrum. In both (a) and (b), the curves are plotted on the same scale to allow quantitative comparison of the signal amplitude for the $\parallel$ and $\perp$ configurations.

together with the corresponding $\parallel$ results. The most striking difference between the two curves is the absence of the dip in the $\perp$ results. This dip is absent for all delay values, resulting in a smooth, photon-echo-like FWM response. In addition, the SO exciton peak is much smaller relative to the continuum contribution.

To understand the experimental results, we have performed simulations of the SR-FWM experiments through numerical integration of the Boltzmann-Bloch equations, in which conduction, heavy-hole, light-hole, and spin-orbit split-off valence bands have been included. Our kinetic equations were derived within a many-body approach, whereby the carrier-carrier Coulomb interaction is included within the screened Hartree-Fock approximation to the self-energy.[18] This approximation gives both mean-field Hartree-Fock contributions to the kinetic equations and scattering terms. However, due to the complexity of the latter in a multiband situation, such phase-breaking scattering processes were treated phenomenologically, as detailed below. The bulk electron wave functions of InP were calculated using $\mathbf{k}\cdot\mathbf{P}$ theory and used to evaluate the Coulomb and electron-light coupling matrix elements explicitly at each electron wave vector. Together with the inclusion of four bulk electron bands, this significantly increases the numerical complexity of our simulations compared with typical jellium model treatments.[2,6,9] The light electric field was taken to consist of two pulses, centered at $t=-\tau$ and $t=0$, with each having an envelope of the form $\mathrm{sech}(1.76t/\tau_p)$. (Here t is the *real* time, τ_p is the pulse duration, and τ is the delay between the two pulses.) The FWM spatial component was extracted from the total calculated polarization by projection.[8]

The effects of exciton-carrier scattering, which are neglected at the Hartree-Fock mean-field level, are treated phenomenologically through the inclusion of a dephasing rate that depends linearly on the total optically excited carrier density:

$$\gamma_v(N_{\rm ex}) = \frac{1}{T_2^v} + \Gamma_v\left(\sum_{\mathbf{k}} f_{c\mathbf{k}}\right). \tag{1}$$

Here $f_{c\mathbf{k}}$ is the conduction band occupation at wave vector $\mathbf{k}$, and v refers to the valence band involved in the interband

transition. This model of exciton-carrier scattering is commonly referred to as EID.[3,9] The rates $1/T_2^v$ take into account dephasing processes associated with phonons and crystal defects, and the EID parameter Γ_v describes the strength of Coulomb-induced exciton-carrier scattering. EID leads to an additional contribution to the FWM polarization at an exciton resonance when a large bandwidth of continuum states is simultaneously excited.[3,9] Such a *continuum contribution*[3,9] to an exciton FWM polarization exhibits the characteristic feature of a rapid decay of the signal amplitude versus delay despite the narrow linewidth of the exciton signal.[3,9] In the simulations, the EID coefficients Γ_v and the non-carrier-related dephasing rates $1/T_2^v$ were varied to provide the best agreement with the experimental data; however, the qualitative features of the numerical results were found to be insensitive to the specific values used. Calculated SR-FWM results are shown in Fig. 2(b). In the calculation, the excitation conditions ($N_{\mathrm{ex}}; \tau_p; E_0$, incident light intensities) were set to the experimental values. Our calculated spectra give excellent agreement with the qualitative features in the experimental data, as seen from a comparison with Fig. 2(a), including the pulse-width limit of the SO exciton peak, the spectral dip, and the peak position of the continuum photon echo with respect to delay. The results in Fig. 2(b) were obtained with dephasing parameter values for the SO to conduction-band transition of $T_2^{\mathrm{so}}=260$ fs, attributed to dephasing by phonons and defects, and $\Gamma_{\mathrm{so}}=5.2\times10^{-20}$ cm^3/fs, in line with the corresponding value at the fundamental exciton of 6.3×10^{-20} cm^3/fs, found by Banyai *et al.*[11] Optimal agreement with the experimental results was found with negligible EID effects in the continuum, suggesting that dephasing processes for continuum transitions 100 meV above the band gap at 1.4×10^{17} cm^{-3} are dominated by non-carrier-related processes, such as optical phonon scattering.[12] The decay rate of the continuum contribution was found to be insensitive to changes in the dephasing time for values lower than $T_2^{\mathrm{HH,LH}}=45$ fs, due to convolution with the pulse profile.

Both the strong SO exciton peak and the sharp dip in the spectra of Fig. 2 are generated by an EID-induced contribution to FWM emission at the SO exciton. This is seen clearly in Fig. 4(a), which shows the calculated FWM spectrum for different strengths of the EID coupling parameter, Γ_{so}. The spectra with no EID effects contains the FPD emission of the SO exciton, which is small due to fast dephasing. The SO exciton signal is only present for temporally overlapped pulses, as apparent in both the experimental and theoretical results of Fig. 2, consistent with an EID-related source.[9] The reduction in the SO exciton signal relative to the continuum emission observed in the experimental results for increasing N_{ex} is also expected for an EID-induced contribution since such a signal is proportional to Γ_{so}, which decreases with carrier density through screening.[6] The EID-induced SO exciton FWM polarization interferes with the continuum polarization, leading to a reduction in the amplitude of the FWM spectrum at low photon energies, an effect which is strongest just below the exciton resonance where it produces the sharp dip seen in Fig. 2. At higher photon energies, the effects of interference are weaker, resulting in a large SO exciton peak.

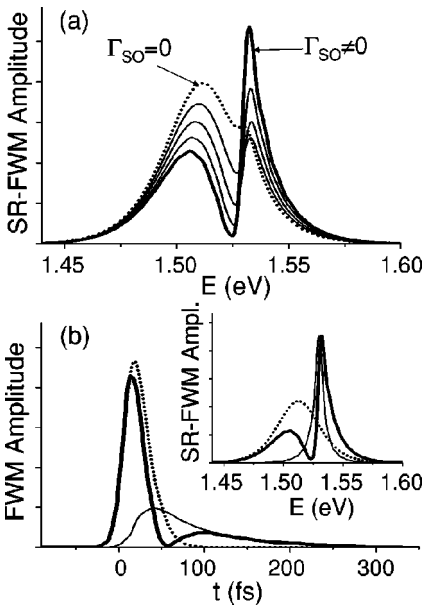

FIG. 4. (a) Calculated FWM spectrum at zero pulse delay for different strengths of the EID coupling. The total dephasing rate of the SO exciton was held constant as Γ_{so} was varied in order to isolate the effects of dephasing from exciton-carrier scattering. Dotted line, $\Gamma_{\mathrm{so}}=0$; thick solid line, $\Gamma_{\mathrm{so}}=6.4\times10^{-20}$ cm^3/fs; thin curves show results for intermediate Γ_{so} values, with equally spaced increments. (b) Calculated FWM polarizations versus real time, *t*, corresponding to the conditions in (a), showing the SO exciton (thin solid curve) and the continuum (dotted curve) polarizations separately, together with the total signal (thick solid curve). For clarity, only the envelopes of the oscillatory polarizations are shown. Inset: FWM spectra corresponding to the time-dependent polarization signals in (b).

The distinct frequency dependence of the interference process between the EID-induced SO exciton and continuum polarizations is a consequence of the *interaction retardation* property of EID-induced signals.[5,9] This property is common to all many-body-induced contributions to FWM, reflecting their origin as polarization scattering emission sources. (FWM sources from noninteracting transitions result from diffraction of the electric field of the second optical pulse from the light-induced carrier population grating, whereas Coulomb-related sources result from diffraction of the *polarization* induced by the second pulse.) The interaction retardation property leads to a slow rise of the SO exciton polarization with time, as seen in Fig. 4(b), where the envelopes of the SO exciton and continuum polarizations are shown together with the envelope of the total polarization. The corresponding spectra appear in the inset. Because of the characteristic slow rise of the EID exciton signal, the impact of interference between the exciton and continuum polarizations on the total signal is time dependent, vanishing for $t<0$ and increasing in importance as t increases. This time-dependent interference efficiency translates in the frequency domain into an asymmetric profile [see Fig. 4(b), inset], where the stronger interference at later times produces the

largest effect at lower frequencies in the spectrum. This interference process is less effective for positive time delay because the pulselike envelope of the continuum polarization, which has the behavior of a photon echo, moves forward in time with increasing delay, τ. As a result, for $\tau>0$ a smaller portion of the continuum envelope overlaps the slow-rise portion of the EID exciton signal, which turns on at $t=0$ (the time of arrival of the second pulse) for all pulse delay values, and the frequency-dependent interference effects are reduced. This accounts for the decrease in the depth of the dip in the spectra of Fig. 2 with increasing pulse delay.

The dramatic spectral features observed when an exciton is excited together with an energetically degenerate continuum allow many-body-induced contributions in SR-FWM to be clearly separated from the noninteracting electric field scattering contribution, or FPD response. Since the frequency-dependent features we observe at the SO exciton are caused by the *interaction retardation* property of many-body related signals, they are not induced by the noninteracting electric field diffraction source terms. An excitonic FPD emission adds symmetrically to an energetically degenerate continuum response in the FWM spectrum. This can be found from a close examination of the numerical results without EID effects [see Fig. 4(a)], and was verified by the authors using a simple two level atom analysis similar to that used by El Sayed *et al*.[9] We have therefore established that many-body effects such as exciton-carrier scattering may be trivially identified at the SO exciton by examining the line shape of the SR-FWM signal, where these effects lead to prominent spectral signatures. Coulomb-mediated effects may therefore be studied at the SO exciton without the need for a series of complex optical experiments, in contrast to coherent experiments at the fundamental exciton where extraction of useful information often necessitates the use of polarization-dependent prepulse FWM and spectrally resolved differential transmission[13,14] or partially nondegenerate FWM.[10] Our finding leads to a dramatic simplification of the interpretation of Coulomb-mediated effects in coherent optical experiments.

Simulations of the FWM experiments were also performed for the $\perp$ geometry. In this polarization configuration, EID-related FWM signals are absent due to a cancellation of contributions from transitions involving electron states with opposite spins.[13,14] Because our treatment included only a single electron spin for each band, EID effects were removed from the $\perp$ simulations to reflect the cancellation of EID sources. This is a good approximation to the full eight-band calculation because the only residual effect of the carrier density dependent dephasing rate is to modify the line shape of the non-EID related contributions to the exciton FWM response, and such contributions are small at the SO exciton. The calculated four-wave mixing spectra at zero delay in the $\parallel$ and $\perp$ geometries are shown in Fig. 3(b). The polarization dependence of SR-FWM emission at the SO band edge are well accounted for by our theoretical model, as seen from comparison with the measured spectra in Fig. 3(a). We note that the calculated spectra for orthogonal polarizations in Fig. 3 are quite similar to the numerical results in the $\parallel$ geometry in the absence of EID effects [see Fig. 4(a), dotted curve]. This result is anticipated since it is known that coherent exchange effects alone do not lead to significant polarization dependence in FWM experiments.[7,14]

We wish to emphasize that, although the FWM spectrum at the SO exciton reported here resembles a Fano resonance,[20,21] Fano effects do not occur. Fano effects arise from quantum interference of coupled discrete and continuum states,[22,23] while in our system the Coulomb coupling of such states is negligible because of the large wave-vector separation of the associated interband transitions ($>500\ \mu\mathrm{m}^{-1}$).

In summary, we have observed the SO exciton in a III-V semiconductor and measured its coherent response using SR-FWM experiments. Our experimental results demonstrate that the energy degeneracy of the SO exciton and heavy-hole and light-hole to conduction band continuum transitions provides a sensitive probe of Coulomb-mediated effects through interference of the FWM emission sources on the separate exciton and continuum transitions. Simulations employing the multiband Boltzmann-Bloch equations including EID provide good agreement with the FWM results.

We gratefully acknowledge the financial support of the Natural Sciences and Engineering Research Council of Canada.

*Present address: DALSA Digital Imaging Solutions, 605 McMurray Road, Waterloo, Ontario, Canada N2V 2E9.

[1] H. Haug and S.W. Koch, *Quantum Theory of the Optical and Electronic Properties of Semiconductors* (World Scientific, Singapore, 1990).
[2] A. Lohner *et al.*, Phys. Rev. Lett. **71**, 77 (1993).
[3] M.U. Wehner *et al.*, Phys. Rev. B **54**, R5211 (1996).
[4] D. Birkedal *et al.*, Phys. Rev. B **54**, R14250 (1996).
[5] D.-S. Kim *et al.*, Phys. Rev. Lett. **69**, 2725 (1992).
[6] M. Lindberg *et al.*, Phys. Rev. B **50**, 18 060 (1994).
[7] T. Rappen *et al.*, Phys. Rev. B **49**, 10 774 (1994).
[8] L. Bányai *et al.*, Phys. Rev. Lett. **75**, 2188 (1995).
[9] K. El Sayed *et al.*, Phys. Rev. B **55**, 2456 (1997).
[10] S.T. Cundiff *et al.*, Phys. Rev. Lett. **77**, 1107 (1996).
[11] L. Bányai *et al.*, Phys. Rev. B **58**, R13341 (1998).
[12] G.R. Allan and H.M. van Driel, Phys. Rev. B **59**, 15 740 (1999).
[13] H. Wang *et al.*, Phys. Rev. Lett. **71**, 1261 (1993).
[14] Y.Z. Hu *et al.*, Phys. Rev. B **49**, 14 382 (1994).
[15] A. Alexandrou *et al.*, Phys. Rev. B **52**, 4654 (1995).
[16] F.X. Camescasse *et al.*, Phys. Rev. Lett. **77**, 5429 (1996).
[17] Q.T. Vu *et al.*, Phys. Rev. B **59**, 2760 (1999).
[18] W. Pötz, Phys. Rev. B **54**, 5647 (1996).
[19] T. Rappen *et al.*, Phys. Rev. B **48**, 4879 (1993).
[20] U. Fano, Phys. Rev. **124**, 1866 (1961).
[21] S. Arlt *et al.*, Phys. Rev. B **58**, 13 073 (1998).
[22] A.R.K. Willcox and D.M. Whittaker, Superlattices Microstruct. **16**, 59 (1994).
[23] S. Glutsch *et al.*, Phys. Rev. B **50**, 17 009 (1994).